

# Meteoric water circulation in a rolling-hinge detachment system (northern Snake Range core complex, Nevada)

Aude Gébelin<sup>1,†</sup>, Christian Teyssier<sup>2</sup>, Matthew T. Heizler<sup>3</sup>, and Andreas Mulch<sup>1,4</sup>

<sup>1</sup>Biodiversity and Climate Research Centre (BiK-F) and Senckenberg, Senckenberganlage 25, 60325 Frankfurt/Main, Germany

<sup>2</sup>Earth Sciences, University of Minnesota, Minneapolis, Minnesota 55455, USA

<sup>3</sup>Bureau of Geology and Mineral Resources, Socorro, New Mexico 87801, USA

<sup>4</sup>Institut für Geowissenschaften, Goethe Universität Frankfurt, Altenhöferallee 1, 60438 Frankfurt/Main, Germany

## ABSTRACT

Combined petrofabric, microstructural, stable isotopic, and <sup>40</sup>Ar/<sup>39</sup>Ar geochronologic data provide a new perspective on the Cenozoic evolution of the northern Snake Range metamorphic core complex in east-central Nevada. This core complex is bounded by the northern Snake Range detachment, interpreted as a rolling-hinge detachment, and by an underlying shear zone that is dominated by muscovite-bearing quartzite mylonite and interlayered micaschist. In addition to petrofabric, microstructural analysis, and <sup>40</sup>Ar/<sup>39</sup>Ar geochronology, we use hydrogen isotope ratios ( $\delta$ D) in synkinematic white mica to characterize fluid-rock interaction across the rolling-hinge detachment. Results indicate that the western flank of the range preserves mostly Eocene deformation (49–45 Ma), characterized by coaxial quartz fabrics and the dominant presence of metamorphic fluids, although the imprint of meteoric fluids increases structurally downward and culminates in a shear zone with a white mica <sup>40</sup>Ar/<sup>39</sup>Ar plateau age of ca. 27 Ma. In contrast, the eastern flank of the range displays pervasive noncoaxial (top-to-the-east) fabrics defined by white mica that formed in the presence of meteoric fluids and yield Oligocene–Miocene <sup>40</sup>Ar/<sup>39</sup>Ar ages (27–21 Ma). Evolution of the Oligocene–Miocene rolling-hinge detachment controlled where and when faulting was active or became inactive owing to rotation, and therefore where fluids were able to circulate from the surface to the brittle-ductile transition. On the western flank (rotated detachment), faulting became inactive early, while continued active faulting on the eastern flank of the detachment allowed surface fluids to reach

the mylonitic quartzite. The combined effects of synkinematic recrystallization and fluid interaction reset argon and hydrogen isotope ratios in white mica until the early Miocene (ca. 21 Ma), when the brittle-ductile transition was exhumed beneath the detachment.

## INTRODUCTION

In most Cordilleran metamorphic core complexes, extensional detachment systems represent the critical interface that separates the cold, brittle upper crust from the ductile middle crust (e.g., Armstrong, 1972; Wright et al., 1974; Coney, 1974, 1980; Miller et al., 1983). This interface is characterized by high shear strain and a sharp metamorphic gradient across it (e.g., Davis and Coney, 1979; Wernicke, 1981; Lister and Davis, 1989; Brun and van den Driessche, 1994). Extensional detachment systems also represent an interface where meteoric and metamorphic fluids interact—a process that is repeatedly documented through the oxygen and hydrogen isotope ratios of synkinematic minerals (e.g., Fricke et al., 1992; Nesbitt and Muehlenbachs, 1995; Losh, 1997; Mulch et al., 2004). This interaction is particularly well recorded in the hydrogen isotopic ratios of synkinematic hydrous minerals within highly sheared detachment footwall rocks (e.g., Mulch et al., 2004, 2005, 2006; Gottardi et al., 2011; Gébelin et al., 2011, 2012, 2013).

Tectonic displacement along these extensional detachment shear zones can induce rapid exhumation of metamorphic footwall rocks and associated hot fluids, while extension and fracturing in the hanging wall generate pathways for downward flow of cold meteoric fluids and upward flow of hot and buoyant fluids. Surface-derived fluids can subsequently be involved in convective flow if three conditions are met (Persson et al., 2007; Gottardi et al., 2013): (1) upper-crustal extension generates fault and fracture

networks with enhanced permeability and porosity; (2) surface topography and relief are sufficiently high to create the necessary hydraulic head; and (3) high geothermal gradients created by exhumation of deep(er) crustal rocks promote buoyancy-driven fluid convection. Therefore, the interplay among surface topography, orographic rainfall, groundwater storage, and heat advection makes detachment systems important orogen-scale structures for fault-controlled hydrothermal activity. In such hydrothermal systems, synkinematic hydrous minerals represent tracers that record and fingerprint the origin of syn-deformational fluids (meteoric, metamorphic, evolved) and permit estimates of time-integrated fluid-rock interaction at various structural levels of the detachment system.

Here, we present combined petrofabric, microstructural, electron backscatter diffraction (EBSD), <sup>40</sup>Ar/<sup>39</sup>Ar thermochronological, and hydrogen isotope ( $\delta$ D) data from mylonitic quartzite exposed across the northern Snake Range detachment footwall. These data provide insight into the spatial and temporal evolution of localized deformation and associated fluid-rock interaction across the detachment, the influence of the dynamics of the detachment system (rolling hinge) on water-rock interaction, and the timing and duration of fluid flow and water-mineral isotopic exchange.

## GEOLOGICAL SETTING AND PREVIOUS WORK

The northern Snake Range detachment defines the Snake Range metamorphic core complex in east-central Nevada (Fig. 1), which resulted from Oligocene–Miocene extension of the Basin and Range Province (Wernicke, 1981; Miller et al., 1983; Bartley and Wernicke, 1984; Gans et al., 1985, 1989; Lee and Sutter, 1991; Lewis et al., 1999; Miller et al., 1999a; Gébelin et al., 2011). The Snake Range metamorphic

<sup>†</sup>E-mail: [aude.gebelin@senckenberg.de](mailto:aude.gebelin@senckenberg.de).

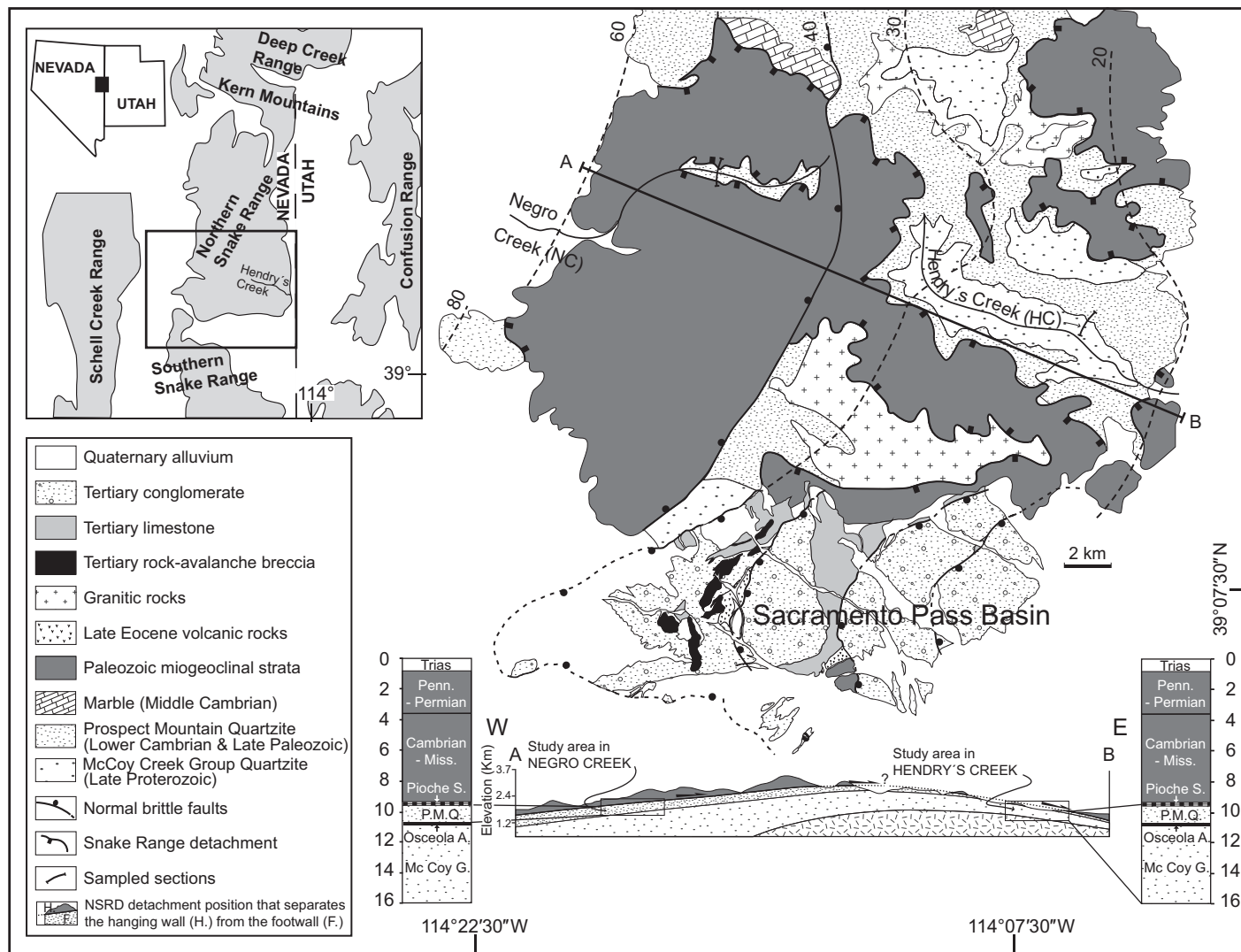


**Figure 1.** Simplified geological map of the southern corner of the northern Snake Range and Sacramento Pass Basin. Solid transect line represents section through the northern Snake Range detachment (NSRD) footwall at Hendry's Creek (HC) and Negro Creek (NC). Schematic geological cross section across the northern Snake Range is modified after Lee and Sutter (1991), showing the structural thickness of lower-plate units after Tertiary ductile thinning. Columns on the left and right of the section represent stratigraphic thickness of metamorphic lower-plate units prior to deformation (Hose and Blake, 1976; Whitebread, 1969; Stewart, 1980). Pioche S.—Pioche Shale; P.M.Q.—Lower Cambrian Prospect Mountain Quartzite; Osceola A.—Osceola Argillite; McCoy G.—Upper Proterozoic McCoy Creek Group.

core complex represents a 150-km-long, north-trending mountain range that extends from the southern Snake Range to the Kern Mountains and Deep Creek Range in the north (Fig. 1) (Gans et al., 1999a, 1999b; Lee et al., 1999a, 1999b, 1999c; Miller and Gans, 1999; Miller et al., 1999b).

The northern Snake Range detachment accommodated top-to-the-east ductile shearing and exhumed metamorphosed Precambrian (McCoy Creek Group) and Cambrian (Prospect Mountain) quartzite and metapelite, as well as Middle Cambrian to Ordovician marble beneath the late Paleozoic and Tertiary unmetamor-

phosed sedimentary rocks of the upper plate (Wernicke, 1981; Lee et al., 1987; Miller et al., 1999a). The amount of extensional displacement has been a topic of considerable debate. Wernicke (1981) interpreted the northern Snake Range detachment as a Cenozoic low-angle normal fault system that accommodated several tens of kilometers of extensional displacement, while other authors have viewed the northern Snake Range detachment as a subhorizontal brittle-ductile transition zone with only limited (<10km) slip (Miller et al., 1983; Gans and Miller, 1983; Gans et al., 1985; Lee et al., 1987; Miller and Gans, 1989; Lee and Sutter, 1991). In

the Wernicke (1981) model, the northern Snake Range detachment cuts out several kilometers of crust and excises at least one major Mesozoic thrust that can be found as a relic in the hanging wall.

Thermobarometric data show that metapelite strata in the footwall were metamorphosed at  $810 \pm 70$  MPa and  $610 \pm 50$  °C, suggesting burial to crustal depths of ~30 km (Lewis et al., 1999). The same authors proposed a kinematic model where Jurassic–Cretaceous crustal shortening was first accommodated by a major west-directed thrust system responsible for tectonic burial. Subsequently, Tertiary unroofing was

achieved by the northern Snake Range detachment in a rolling-hinge fashion (Lee, 1995), where a steeply dipping large-scale listric fault in the upper 8 km crustal segment flattens to a dip of  $\sim 15^\circ$  at a depth of 12–18 km, accommodating up to 50 km of eastward displacement of hanging-wall rocks (Lewis et al., 1999).

In an alternative model (Miller et al., 1983; Lee et al., 1987), the northern Snake Range detachment separates a brittlely extended (450%) upper plate from an equally stretched lower plate. Based on the observation that there is no structural repetition or omission of stratigraphic sections across the northern Snake Range detachment, these authors proposed a small displacement of up to  $\sim 10$  km. They also described a strong west-to-east increase in strain intensity accompanied by a dominant top-east shearing and suggested that the shear zone evolved from dominantly coaxial strain to noncoaxial strain, which is best exemplified on the eastern flank of the northern Snake Range detachment.

Using previous (Armstrong and Hansen, 1966; Lee et al., 1970, 1980, 1987) and new  $^{40}\text{Ar}/^{39}\text{Ar}$  thermochronology data, Lee and Sutter (1991) highlighted a systematic decrease in  $^{40}\text{Ar}/^{39}\text{Ar}$  ages from ca. 80 Ma on the west flank of the Snake Range metamorphic core complex to ca. 20 Ma on the east flank, and they suggested that rock units in the east record prolonged residence at higher temperature. Further modeling of  $^{40}\text{Ar}/^{39}\text{Ar}$  data indicates that the western flank of the range cooled below  $300^\circ\text{C}$  at ca. 49–45 Ma, while the east remained at temperatures above  $300^\circ\text{C}$  until ca. 19 Ma (Lee, 1995). Based on these relationships, Lee (1995) proposed that the northern Snake Range detachment acted as a rolling-hinge detachment that rotated from steep ( $>40^\circ$ ) to shallow ( $10^\circ$ – $20^\circ$ ) dips in response to exhumation by isostatic unloading of the footwall.

The initiation of northern Snake Range detachment activity is thought to have occurred in the latest Eocene, with contemporaneous lower-crustal flow and upwelling of rocks followed by significant slip on the detachment and ultimate unroofing of the lower plate in the middle Miocene (ca. 17 Ma; Miller et al., 1999a). This last stage of slip accommodated at least 12 km of displacement (Miller et al., 1999a) and overprinted a preexisting Oligocene–Miocene mylonitic fabric associated with hydrothermal activity (Gébelin et al., 2011).

There is general agreement that the northern Snake Range detachment juxtaposes a lower-grade hanging wall against a higher-grade underlying metamorphic footwall and that this underlying footwall contains a top-to-the-east mylonitic shear zone that exposes a few hun-

dred meters of muscovite-bearing quartzite mylonite and schist. During the late Oligocene and early Miocene, deuterium-depleted (low- $\delta\text{D}$ ) meteoric fluids infiltrated this zone of high strain, as recorded by the hydrogen isotope composition of recrystallized muscovite grains (Gébelin et al., 2011). Recrystallized muscovite and quartz grains define a strong foliation containing mineral and stretching lineations that are particularly well developed at Hendry's Creek (HC; Fig. 1).

#### NORTHERN SNAKE RANGE DETACHMENT SHEAR ZONE: STRUCTURE AND INTERNAL DEFORMATION

The southern part of the northern Snake Range provides excellent exposure of the northern Snake Range detachment footwall, composed almost entirely of sheared quartzite and interlayered schist units (e.g., Lee et al., 1987; Lee and Sutter, 1991; Miller et al., 1999a) in the Hendry's Creek and Negro Creek areas, located on the eastern and western flanks of the range, respectively (Fig. 1). The deepest levels of lower-plate mylonite crop out at Hendry's Creek and consist of an  $\sim 300$ -m-thick structural section of muscovite-bearing quartzite and mica schist, which are part of a metamorphosed Late Precambrian to early Mesozoic shelf-facies sequence (Hose and Blake, 1976; Whitebread, 1969; Stewart, 1980). Shallower levels are exposed to the west of the range in Negro Creek, where deformed quartzite can be observed over  $\sim 160$  m of structural thickness. Owing in part to the lack of continuity of quartzite exposure from east to west and a likely difference of structural depth variation within the northern Snake Range detachment footwall, the relationship between deformed rocks on either side of the metamorphic core complex is not straightforward.

#### Hendry's Creek

The northern Snake Range detachment footwall is particularly well exposed at Hendry's Creek, with more than 300 m of Lower Cambrian (Prospect Mountain) and Upper Proterozoic (McCoy Creek) quartzite and schist (Fig. 1). The Prospect Mountain Quartzite and the Pioche Shale, which locally appears above, form the top 60 m of the section and overlie the McCoy Creek Group fine- to coarse-grained quartzite and staurolite-garnet-bearing schist. These rocks are overprinted by a mylonitic fabric and contain a shallowly E-dipping foliation and a WNW-ESE-trending mineral lineation.

Synkinematic muscovite grains collected systematically over 300 m of section within the

detachment footwall reveal Oligocene–Miocene  $^{40}\text{Ar}/^{39}\text{Ar}$  ages that become increasingly younger from top to bottom (26.9 Ma to 21.3 Ma; Gébelin et al., 2011). The same minerals show  $\delta\text{D}_{\text{muscovite}}$  values as low as  $-150\text{‰}$  at the top of the detachment zone and attain progressively higher values of up to  $-72\text{‰}$  at the bottom of the section (see following). This general trend is disrupted at two depth intervals (15–25 m and 91–144 m), where  $\delta\text{D}_{\text{muscovite}}$  increases rapidly to high values ( $\sim -70\text{‰}$ ). The low  $\delta\text{D}_{\text{muscovite}}$  values within the uppermost northern Snake Range detachment footwall mylonite are consistent with recrystallization of muscovite in the presence of meteoric water, with calculated  $\delta\text{D}_{\text{water}}$  values of  $-113\text{‰}$   $+12/-11\text{‰}$  at the inferred temperature of ductile deformation and isotopic equilibration of  $402 \pm 52^\circ\text{C}$  (Gébelin et al., 2011). The hydrogen isotope pattern correlates with quartz microstructures (Fig. 2) that are characterized by very fine-grained neoblasts showing subgrain rotation at the top of the detachment (Figs. 2E and 2F), and a coarser quartz fabric characterized by grain boundary migration toward the bottom of the section (Figs. 2G and 2H). The quartz *c*-axis fabric is defined by a strong maximum parallel to *Y* and a single girdle shape that stretches into an inclined girdle, the pole of which is the largest concentration of *a* axes, consistent with top-to-the-east shearing (Fig. 2). Quartz *c*-axis and *a*-axis fabrics are constant from the top to the base of the section. These data are compatible with plastic deformation dominated by prism-a glide that typically occurs at temperatures above  $350$ – $400^\circ\text{C}$  (Tullis et al., 1973; Mainprice and Paterson, 1984).

The fabric strength for Hendry's Creek samples was investigated using the J index (Bunge, 1982) for the *c*-axis (Jc) and *a*-axis (Ja), as well as the P, G, and R indices of *c*-axis distributions (e.g., Vollmer, 1990; Ulrich and Mainprice, 2005), using PFch5 (Mainprice, 2005; Fig. 3; Supplementary Table DR1<sup>1</sup>). The magnitude of those indices indicates whether the crystallographic preferred orientation defines a point (P), a girdle (G), or a random (R) distribution (R = 1 indicates the absence of a preferred orientation). In a ternary PGR diagram (Abalos, 1997), the

<sup>1</sup>GSA Data Repository item 2014281, Table DR1 (strength of the lattice preferred orientation), Table DR2 (microstructural analysis results using EBSD software), Table DR3 ( $^{40}\text{Ar}/^{39}\text{Ar}$  thermochronology results), Table DR4 (hydrogen isotope results, Negro Creek), Table DR5 (hydrogen isotope results, Hendry's Creek), Table DR6 (muscovite compositions), Text DR1 (electron backscatter diffraction method and analytical procedure), Text DR2 ( $^{40}\text{Ar}/^{39}\text{Ar}$  thermochronology analytical procedure), Text DR3 (hydrogen isotope analytical method), is available at <http://www.geosociety.org/pubs/ft2014.htm> or by request to [editing@geosociety.org](mailto:editing@geosociety.org).

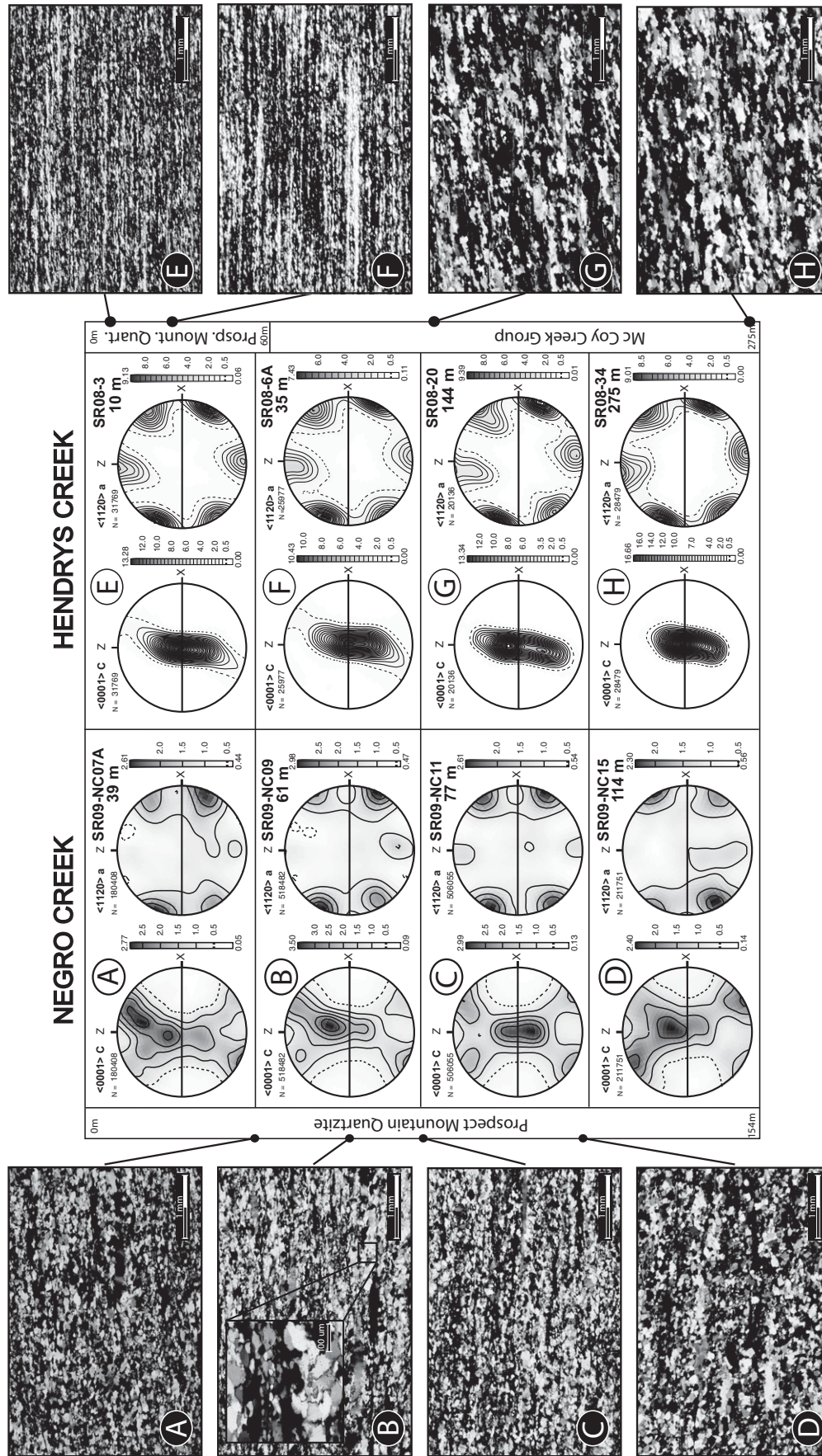
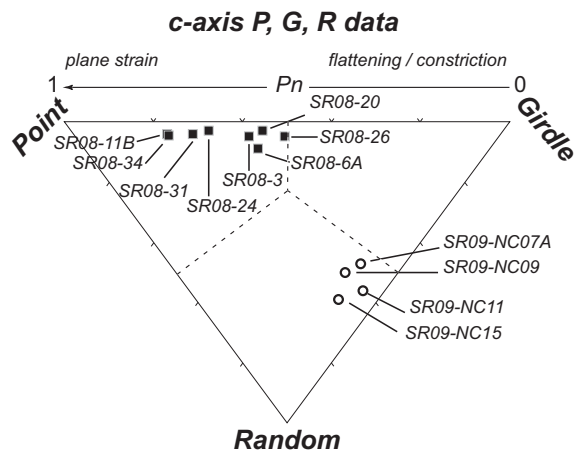


Figure 2. Electron backscatter diffraction quartz microstructures and lattice preferred orientation of mylonitic quartzite from Negro Creek and Hendry's Creek. Equal-area projection, lower hemisphere. Foliation (X-Y plane) is vertical, and lineation (X) is horizontal in this plane. Note that quartzite at Negro Creek experienced a strong coaxial deformation, while at Hendry's Creek, a top-to-the-east noncoaxial strain characterizes rocks in the northern Snake Range detachment footwall.

**Figure 3.** Vollmer diagram based on quartz lattice preferred orientation showing a clear difference between quartzite fabrics from Negro Creek and Hendry's Creek (see text for details).



samples cluster in the high P ( $0.48 < P < 0.75$ ) and medium G ( $0.22 < G < 0.47$ ) segment. R indices are very low ( $0.03 < R < 0.09$ ). The corresponding Jc index, which ranges between 4.87 and 8.23, reveals a high fabric strength (Supplementary Table DR1 [see footnote 1]).

### Negro Creek

Mylonitic quartzite and schist that comprise Lower Cambrian Prospect Mountain Quartzite and Pioche Shale were collected across ~160 m of section (sample spacing ~10 m) at Negro Creek on the western flank of the Snake Range (Fig. 1). The primary thickness before Mesozoic

metamorphism and Tertiary extension is estimated at ~1200 m (Prospect Mountain quartzite) and ~120 m (Pioche Shale; Fig. 1; Hose and Blake, 1976; Whitebread, 1969; Stewart, 1980). Currently, the entire section has been tectonically thinned (160 m), with minimum structural thickness further east (60 m) in Hendry's Creek (Fig. 1).

The Prospect Mountain Quartzite at Negro Creek consists of light-gray to white layers that display well-preserved cross-stratification. These beds are occasionally interlayered with discontinuous, up to 50-cm-thick schist intervals. The quartzite and schist exhibit shallowly W-dipping foliation and WNW-trending min-

eral lineation. Thinly bedded calcareous quartzite and dark-colored siltstone of the Pioche Shale form the top 20 m of the studied section. This unit represents an important lithologic transition with the overlying Middle Cambrian limestone (Fig. 1). Based on the contrast in their internal deformation style and metamorphic grade, Lee and Sutter (1991) placed the northern Snake Range detachment at the top of the Pioche Shale (Fig. 1). The Osceola Argillite and McCoy Creek Group, which underlie the Prospect Mountain Quartzite, are both well exposed at Hendry's Creek but do not crop out in Negro Creek (Fig. 1). As a result, the 160 m thickness of Prospect Mountain Quartzite at Negro Creek represents a minimum estimate.

We investigated quartz microfibrils of representative quartzite samples by EBSD (Fig. 2; analytical procedure in supplementary text 1 [see footnote 1]). These samples are distributed over the exposed part of the northern Snake Range detachment footwall, with the top of the section, i.e., the contact with the hanging wall, as reference level (Lee and Sutter, 1991). Quartz microstructures in the Prospect Mountain Quartzite are similar across the section (Fig. 2). They are characterized by large relict quartz grains (~5%–10%), recrystallized large quartz grains (30%–50%), and fine-grained recrystallized quartz within the quartz-mica matrix (>50%; Figs. 2 and 4). Relict grains are elongate or ribbon-like ( $\geq 1000 \times 120 \mu\text{m}$ ) and define the

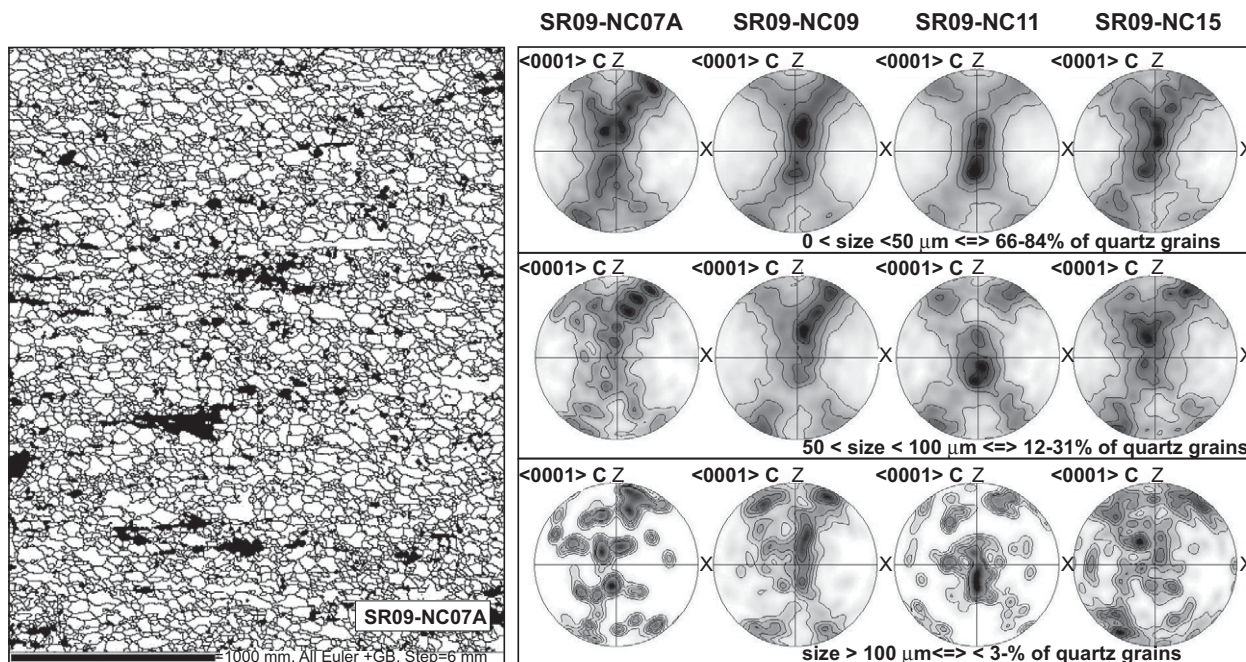


**Figure 4.** Right: Quartz *c*-axis fabrics plotted against different quartz grain sizes ( $0 < \text{size} < 50 \mu\text{m}$ ,  $50 < \text{size} < 100 \mu\text{m}$ ,  $\text{size} > 100 \mu\text{m}$ ) for samples collected at Negro Creek. Left: Mapping of subgrains and recrystallized grains for sample SR09-NC07A.

macroscopic foliation (Figs. 2A, 2B, and 2C), which is also defined by shearing surfaces and mica fish. Quartz ribbons display undulatory extinction (Fig. 2A), contain deformation lamellae and recrystallized new grains ranging from 50 to 100  $\mu\text{m}$  in diameter, and are surrounded by small recrystallized grains (<30  $\mu\text{m}$ ) along grain margins. Recrystallized quartz grains in the matrix vary from 10 to 50  $\mu\text{m}$  in size and are clumped together or distributed along shear bands oblique ( $15^\circ$ – $40^\circ$ ) to the macroscopic foliation (Figs. 2 and 4). “Castellate” microstructures and “leftover grains” (Jessell, 1987; Fig. 2B) indicate recrystallization dominated by grain boundary migration.

Quartz *c*-axis fabrics correspond to type-I cross-girdle patterns (Figs. 2A, 2B, 2C, and 2D; Lister, 1977). Three fabric subtypes can be distinguished: The *c*-axis maxima in the first fabric subtype are located at positions between *Y* and *Z*, suggesting operation of rhomb  $\langle a \rangle$  slip (Figs. 2A and 2B). In this case, the *a*-axes are asymmetrically distributed with respect to the lineation and cluster in a point maximum at  $\sim 25^\circ$  to the shear plane, consistent with top-to-the-east sense of shear. The second fabric subtype displays a symmetric density distribution of *c*-axis maxima about the macroscopic strain axes (Fig. 2C). In this case, the *c*-axis maxima are located along *Y*, suggesting that prism and rhomb  $\langle a \rangle$  were the dominant slip systems, and the *a*-axis maxima are distributed nearly symmetrically, indicating a strong coaxial component during ductile deformation. In the third fabric subtype, the quartz *c* axes define a great-circle girdle with submaxima that indicate almost equal components of basal, prism, and rhomb  $\langle a \rangle$  slip. The corresponding *a* axes are concentrated in a maximum at  $20^\circ$ – $25^\circ$  to the macroscopic foliation, indicating top-to-the-west sense of shear (Fig. 2D).

We used the EBSD software to define quartz grain boundaries ( $>10^\circ$  misorientation) and measure grain sizes in the samples for which the fabric is described here. Results within the top 80 m of the detachment footwall indicate that  $\sim 83\%$  of the quartz grains (interpreted as dynamically recrystallized new grains) have a size smaller than 50  $\mu\text{m}$ ,  $\sim 15\%$  range between 50 and 100  $\mu\text{m}$ , and only  $\sim 1\%$  are larger than 100  $\mu\text{m}$  (Fig. 4; Supplementary Table DR2 [see footnote 1]).

The calculated surface areas indicate two equally represented main populations ( $\sim 45\%$  each), except for one sample located at the bottom of the section, which displays a slightly different distribution, with medium grains (50–100  $\mu\text{m}$ ) covering 54% of the surface, while the smallest and largest grains represent 29% and 17%, respectively (Supplementary Table DR2 [see footnote 1]). Although the microstructures

of these four samples display some differences, there is no clear correlation between the distribution of quartz *c*-axis fabrics and quartz grain size (Fig. 4).

On the ternary PGR Vollmer diagram (Fig. 3; Supplementary Table DR1 [see footnote 1]), the Negro Creek samples cluster in the very low P ( $0.05 < P < 0.12$ ) and medium G ( $0.32 < G < 0.43$ ) and R ( $0.47 < R < 0.59$ ) region. The corresponding *Jc* index ranges between 1.31 and 1.50 and indicates that the fabric is weak to moderate (Supplementary Table DR1 [see footnote 1]). In summary, quartz fabrics at Negro Creek bear moderate strengths from the top to the base of the section and indicate a large component of coaxial deformation.

### Microstructural Differences between Hendry's Creek and Negro Creek

Comparison of Negro Creek quartz microstructure and crystallographic preferred orientation to those at Hendry's Creek indicates that quartzite from the two areas did not experience the same type of deformation: (1) The *J* index at Negro Creek has low values ( $1.31 < Jc < 1.50$ ) when compared to Hendry's Creek ( $4.87 < Jc < 8.23$ ) (Fig. 3; Supplementary Table DR1 [see footnote 1]). (2) In contrast to Negro Creek samples displaying cross girdles indicative of coaxial deformation, Hendry's Creek quartz *c*-axis fabrics are characterized by oblique partial single girdles indicating top-to-the-east shear (Figs. 2E, 2F, 2G, and 2H). (3) In contrast to quartz microstructures at Negro Creek that are similar across the section, those observed from Hendry's Creek samples vary from top to bottom of the section and record different dislocation creep regimes (Hirth and Tullis, 1992), from subgrain rotation to grain boundary migration, and recrystallized quartz grain size increases from 5 to  $>200$   $\mu\text{m}$  from the top to the bottom of the section (Figs. 2E, 2F, 2G, and 2H). (4) Recrystallized quartz grains from samples within the top 60 m of the Hendry's Creek section are elongate obliquely ( $\sim 25^\circ$ ) to the macroscopic foliation, in agreement with top-to-the-east sense of shear.

### $^{40}\text{Ar}/^{39}\text{Ar}$ GEOCHRONOLOGY OF NEGRO CREEK QUARTZITE

#### Muscovite Microstructure and Chemical Composition

Muscovite within the top  $\sim 120$  m of section at Negro Creek exhibits lozenge-shape grains (group 2 of Ten Grotenhuis et al., 2003; Figs. 5A, 5B, and 5C). Their long axes ( $\geq 150$   $\mu\text{m}$ ) are inclined at an angle of  $\sim 25^\circ$  to the shear plane.

Cleavage planes are locally sigmoidal and converge at both tips of the mica grain. When isolated, trails extending from oblique mica fish form stair-stepping patterns in agreement with top-to-the-east sense of shear. Most of these lenticular mica fish display intense recrystallization of small muscovite grains along their rims and in pressure shadows but are devoid of intragrain deformation features, such as kink bands or microfractures. Based on their shape, it is likely that the mica fish and associated fine-grained muscovite tails formed by solution precipitation (Wilson and Bell, 1979; Dunlap, 1992). No significant difference in chemical composition is observed in muscovite samples collected in the top  $\sim 120$  m of the northern Snake Range detachment footwall quartzite (Fig. 6; Supplementary Table DR6 [see footnote 1]).

In contrast, muscovite microstructures from sample SR09-NC18, located in the deepest part of the Negro Creek section (154 m), are distinctly different (Fig. 5D). Muscovite grains are large ( $\geq 1000$  by 300  $\mu\text{m}$ ) and lenticular and display cleavage planes at an angle of  $\sim 40^\circ$  to the shear plane. Whereas cleavage planes can be sigmoidal and converge at the tips of the grain (group 2 of Ten Grotenhuis et al., 2003), there is a significant fraction of grains where cleavage planes are kinked, as observed in rhomboidal shaped fish (group 4 of Ten Grotenhuis et al., 2003). Small muscovite grains commonly surround these large grains (Fig. 5D). The chemical composition of both small and large muscovite grains differs from muscovite collected within the uppermost 120 m of the Negro Creek transect. The latter is characterized by low  $\text{Al}^{\text{VI}}$  and high  $\text{Mg} + \text{Fe}_{\text{total}}$  contents, whereas the former (e.g., SR09-NC18) reveals higher  $\text{Al}^{\text{VI}}$  and lower  $\text{Mg} + \text{Fe}_{\text{total}}$  contents, similar to muscovite present at Hendry's Creek (Gébelin et al., 2011; Fig. 6).

#### $^{40}\text{Ar}/^{39}\text{Ar}$ Geochronology

Furnace step-heating  $^{40}\text{Ar}/^{39}\text{Ar}$  geochronology of multigrain muscovite separates within the top 120 m of Negro Creek footwall mylonite yielded disturbed age spectra that show a monotonous rise in apparent  $^{40}\text{Ar}/^{39}\text{Ar}$  ages in the low-temperature release steps, followed by a “saddle”-shaped release spectrum at higher temperatures (Fig. 5; supplementary Table DR3 and text 2 [see footnote 1]). Integrated  $^{40}\text{Ar}/^{39}\text{Ar}$  ages of muscovite fish from samples SR09-NC7A (39 m), SR09-NC11 (77 m), and SR09-NC15 (114 m) are  $47.7 \pm 0.1$  Ma,  $44.7 \pm 0.1$  Ma, and  $48.8 \pm 0.1$  Ma, respectively (Figs. 5A, 5B, and 5C). In contrast, sample SR09-NC18 (at 154 m) provides a plateau age of  $26.8 \pm 0.1$  Ma, which includes  $>95\%$  of  $^{39}\text{Ar}$  released (Fig. 5D).

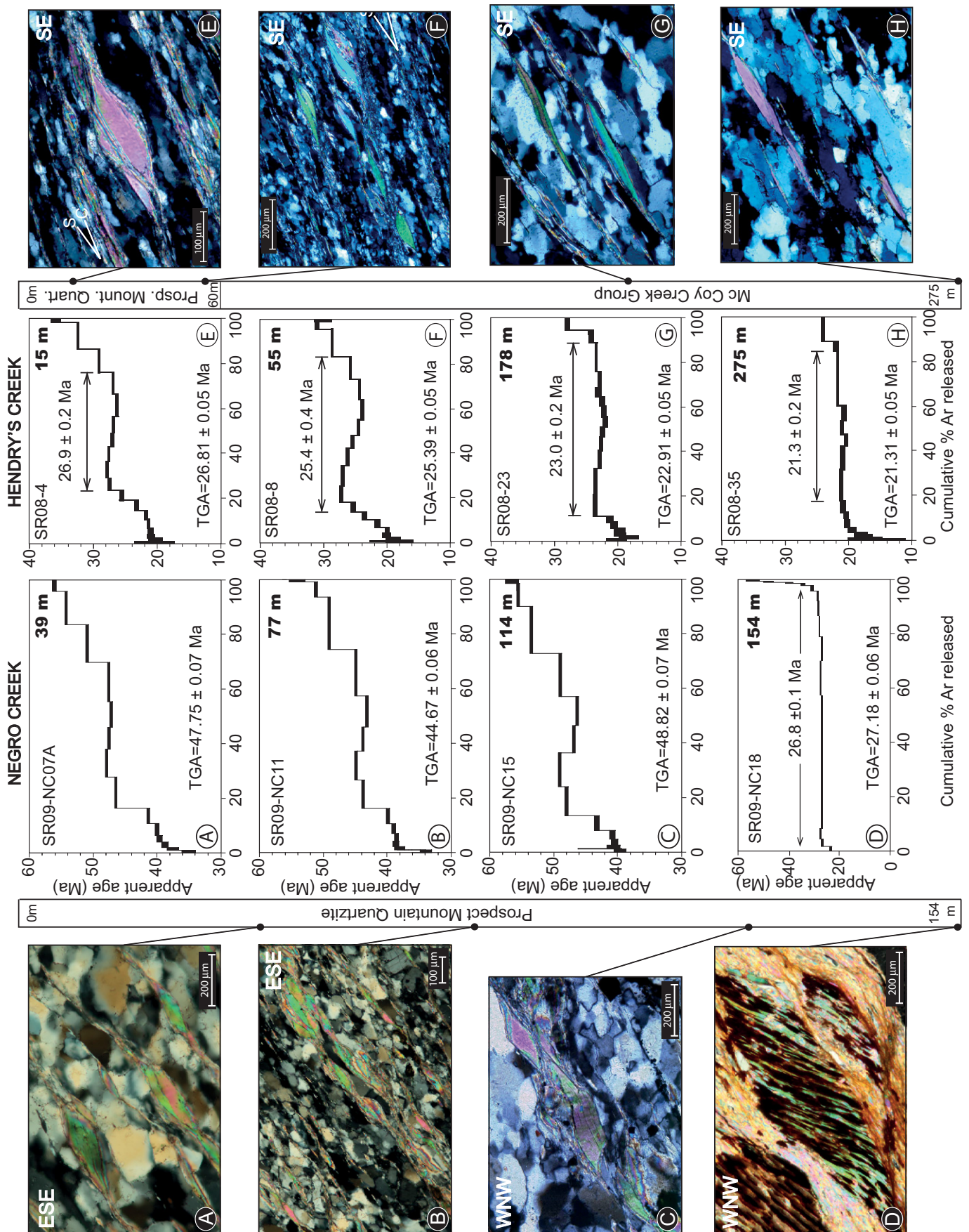
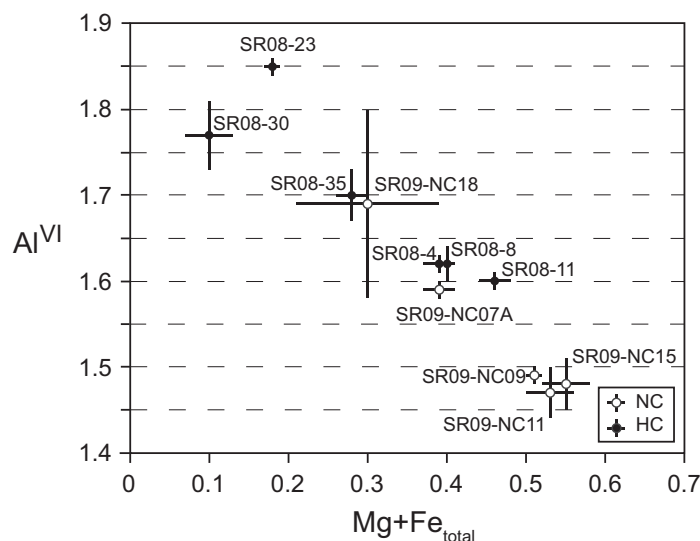


Figure 5.  $^{40}\text{Ar}/^{39}\text{Ar}$  step-heating spectra of muscovite fish and muscovite microstructure from samples collected at Negro Creek (left) and Hendry's Creek (right). TGA—total gas age.



**Figure 6.**  $Al^{VI}$  vs.  $Mg + Fe_{total}$  of muscovite from the eastern and western flanks of the northern Snake Range metamorphic core complex. See muscovite compositions on Table DR6 (see text footnote 1) for Negro Creek samples and Gébelin et al. (2011) for Hendry's Creek samples.

#### HYDROGEN ISOTOPE GEOCHEMISTRY OF NEGRO CREEK QUARTZITE

Muscovite  $\delta D$  values were analyzed in 14 samples of mylonitic quartzite and schist collected over ~160 m of section beneath the northern Snake Range detachment at Negro Creek (Fig. 7; Supplementary Table DR4 and analytical procedures in supplementary text 3 [see footnote 1]). Muscovite shows high  $\delta D$  values, ranging from  $-64\%$  to  $-86\%$  at the top of the section, and attains progressively lower values (down to  $-142\%$ ) toward the base of the section (all values with respect to standard mean ocean water [SMOW]). The high  $\delta D_{muscovite}$  values at the top of the section fall in the range of metamorphic muscovite and are associated with mica schist as the dominant rock type (Pioche Shale). Going down section,  $\delta D_{muscovite}$  values iterate between high and low values, with progressively more negative values toward the bottom of the section, indicating an increasingly strong interaction with meteoric fluids, most likely sourced at high elevation (e.g., Taylor, 1990).

The lowest  $\delta D_{muscovite}$  value at the base of the Negro Creek section ( $-142\%$ ; sample SR09-NC18) is similar to those measured at the top of the Hendry's Creek section, where, in contrast to Negro Creek,  $\delta D_{muscovite}$  values become less negative from the top ( $\delta D \sim -150\%$ ) to the bottom of the section ( $\delta D \sim -70\%$ ) (see previous section; Fig. 7; Supplementary Table DR5 [see footnote 1]).

#### DISCUSSION

The northern Snake Range metamorphic core complex has several important attributes for evaluating the role of fluids during Cenozoic extension: (1) The upper crust experienced a large amount of extension ( $>450\%$ ) (Miller et al., 1983). (2) The emplacement of Cenozoic (ca. 40–20 Ma) crustal melts advected heat toward shallow levels of the crust (Gans and Miller, 1983; Miller et al., 1988; Gans et al., 1989; Miller et al., 1999a). (3) The Snake Range most likely represented a topographic high during the Oligocene–Miocene (Gébelin et al., 2012). (4) The mylonitic quartzite for which the stratigraphy is well known (Whitebread, 1969; Hose and Blake, 1976; Stewart, 1980) is mineralogically simple and constitutes the main lithology of the mylonitic detachment footwall.

Microstructural, stable isotopic, and geochronologic data from quartzite collected along the western and eastern flanks of the range highlight two distinct metamorphic and kinematic Cenozoic events. First, quartz  $c$ -axis fabric patterns reveal a large component of coaxial strain in quartzite from Negro Creek, whereas rocks from Hendry's Creek reveal a consistent top-to-the-east sense of shear (Fig. 2). Second, hydrogen isotope ratios in muscovite from Negro Creek quartzite are shifted toward low values going down section, in contrast to Hendry's Creek, where values increase from the top to the base of the section (Fig. 7). Third, elemental compositions reveal distinct muscovite popu-

lations with lower  $Al^{VI}$  and higher  $Mg + Fe_{total}$  contents for muscovite collected at Negro Creek (Fig. 6). Fourth, although most samples display some degree of disturbance,  $^{40}Ar/^{39}Ar$  ages obtained along the western flank of the range (except SR09-NC18) yield Eocene ages (ca. 49–45 Ma), whereas those from the east provide Oligocene–Miocene ages (ca. 27–21 Ma).

#### Interpretation of $\delta D_{muscovite}$

Muscovite  $\delta D$  values from the western and eastern flanks of the northern Snake Range indicate that the quartzite experienced different syndeformational fluid-flow histories. Muscovite from Hendry's Creek shows a trend from low  $\delta D$  values within the top 83 m of section ( $\sim -150\%$ ), typical for meteoric fluids, to high values towards the bottom ( $\sim -70\%$ ; Fig. 7; Supplementary Table DR5 [see footnote 1]). In contrast, muscovite from Negro Creek displays high  $\delta D$  values at the top of the section ( $> -85\%$ ) that gradually decrease to low values toward the bottom of the section ( $< -140\%$ ; Fig. 7; Supplementary Table DR4 [see footnote 1]). The lowest observed  $\delta D_{muscovite}$  values at Negro Creek (SR09-NC11, 77 m,  $\sim -124\%$ ; SR09-NC15, 114 m,  $-130\%$ ; SR09-NC18, 154 m,  $-142\%$ ) require interaction with meteoric water (e.g., Fricke et al., 1992; Mulch et al., 2006). Previous studies in the same area estimated temperatures of deformation between 300 °C and 450 °C (Lee et al., 1987; Lee, 1995; Gébelin et al., 2011). Using a temperature estimate of  $375 \pm 75$  °C, appropriate hydrogen isotope muscovite-water fractionation parameters (Suzuoki and Epstein, 1976), and measured  $\delta D_{muscovite}$  values of these four samples,  $\delta D_{water}$  values present during recrystallization of muscovite from these three samples were  $-90\%$  to  $+14\%$ – $-11\%$ ,  $-96\%$  to  $+14\%$ – $-11\%$ , and  $-108\%$  to  $+14\%$ – $-11\%$ , respectively. The  $\delta D_{water}$  values as low as  $-108\%$  to  $+14\%$ – $-11\%$  (SR09-NC18) at Negro Creek are in good agreement with  $\delta D_{water}$  calculated from mylonitic quartzite in the Hendry's Creek section indicating strong time-integrated water-rock interaction with low- $\delta D$  meteoric fluids ( $\leq -115\% \pm 5\%$ ; Gébelin et al., 2011).

#### Interpretation of $^{40}Ar/^{39}Ar$ Data

To determine the timing of meteoric water–muscovite hydrogen isotope exchange, we used  $^{40}Ar/^{39}Ar$  thermochronology on Negro Creek samples with low (SR09-NC11, SR09-NC15, and SR09-NC18) and high (SR09-NC07A)  $\delta D_{muscovite}$  values. Even though first-release steps display early Oligocene apparent ages in the age spectrum, samples within the 0–120 m section interval yield relatively simi-



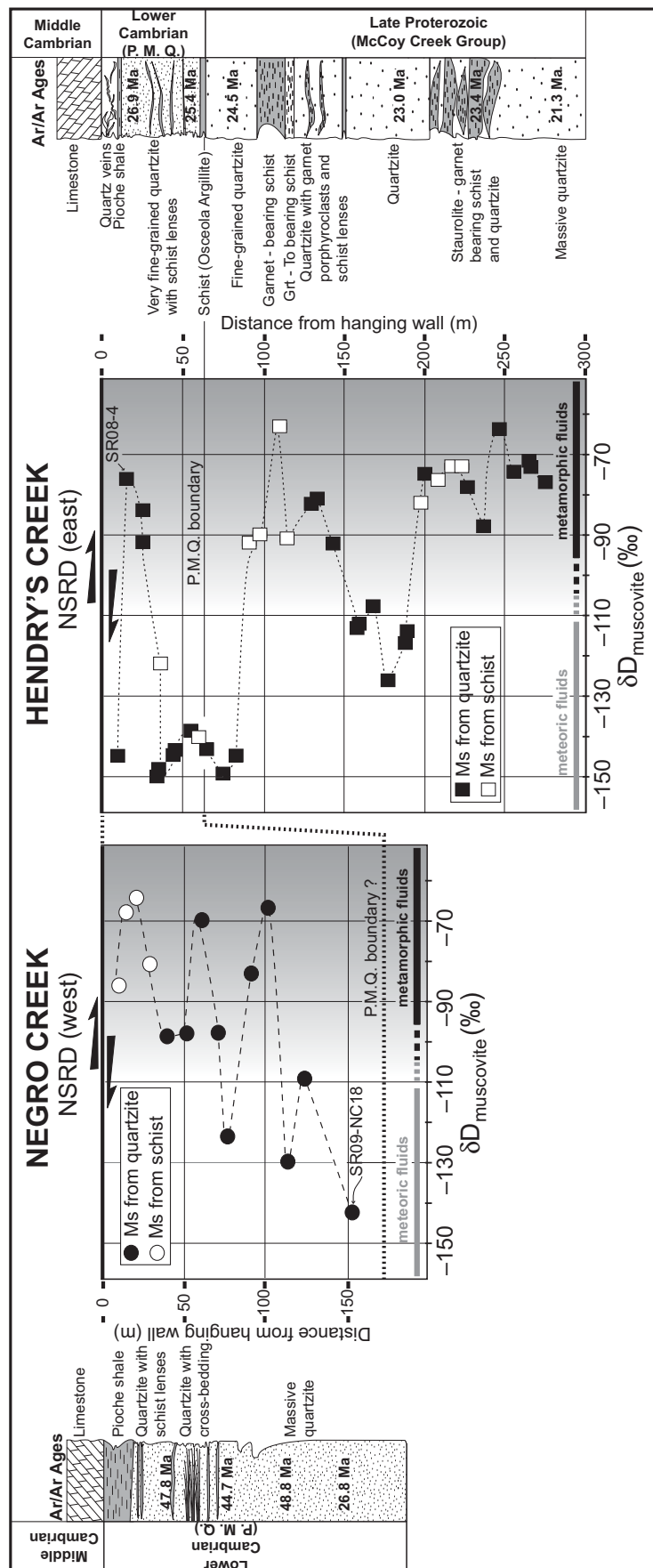


Figure 7.  $\delta D$  values of muscovite (Ms) from quartzite in the footwall of the northern Snake Range detachment (NSRD) at Hendry's Creek and Negro Creek. P.M.Q.—Prospect Mountain Quartzite.

lar, yet complex spectra with Eocene total gas ages of ca. 49–45 Ma (Fig. 5). Similar results were reported by Lee and Sutter (1991), who attributed the low-temperature steps to a thermal event (e.g., intrusion of ca. 37 Ma rhyolite porphyry dikes) that led to partial degassing of  $^{40}\text{Ar}$  from these muscovites. These authors considered the 46 Ma to 58 Ma high-temperature steps to represent a minimum estimate for muscovite closure to argon diffusion ( $\sim 325^\circ\text{C}$ ) subsequent to Late Cretaceous peak metamorphic temperature conditions.

The observed constant orientation of foliation and lineation, microstructures, and *c*-axis fabrics reflect early Eocene pure shear-dominated deformation associated with collapse of the Sevier thrust belt (Lewis et al., 1999). The different quartz grain sizes displaying similar fabrics suggest that all quartz grains heterogeneously recrystallized during this coaxial deformational event (Fig. 4). Asymmetric/sigmoidal mica fish, shear bands, and muscovite tails indicate that muscovite most likely recrystallized by combined dissolution/precipitation and migration recrystallization in a recrystallized quartz matrix during deformation (Fig. 2). Furthermore, no trend in intragrain muscovite composition is detected from the core to tip, suggesting that muscovite grew during the same Eocene deformation event (Supplementary Table DR6 [see footnote 1]). Eocene recrystallization of muscovite is also supported by elongated muscovite from deformed pegmatite and aplite bodies collected along the western part of the range that yield plateau ages of ca. 48 Ma (Lee and Sutter, 1991).

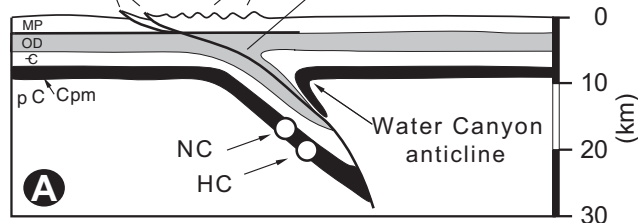
The 49–45 Ma  $^{40}\text{Ar}/^{39}\text{Ar}$  ages within the top 120 m of section may represent progressive cooling owing to exhumation after Cretaceous tectonic burial (Fig. 8). The observed saddle-shaped spectra reflect the combined effects of synkinematic white mica growth, cooling-related closure to  $^{40}\text{Ar}$  diffusion, and/or mixing of different white mica populations owing to various degrees of recrystallization of Cretaceous muscovite in the respective samples. In contrast, sample SR09-NC18, collected at the bottom of the section, yields a  $^{40}\text{Ar}/^{39}\text{Ar}$  plateau age of ca. 27 Ma. This age is, within error, identical to the  $^{40}\text{Ar}/^{39}\text{Ar}$  ages at the top of the Hendry's Creek section (Fig. 5). Muscovites from SR09-NC18 are large and kinked and, in contrast to samples within the 0–120 m section interval at Negro Creek, have chemical compositions that fall into the segment of Al-rich muscovite (Fig. 6). This sample, with a perfect late Oligocene plateau age, a low  $\delta D_{\text{muscovite}}$  value, and an Al-rich muscovite composition, therefore, shares similar features with samples from the top of the Hendry's Creek section.

Figure 8. Kinematic model of Jurassic–Cretaceous crustal shortening and Tertiary unroofing (after Lewis et al., 1999). MP—Mississippian through Permian strata; OD—Ordovician through Devonian strata; C—Cambrian strata; Cpm—Prospect Mountain Quartzite; pC—Precambrian; NC—Negro Creek section; HC—Hendry’s Creek section. (A) West-directed thrust system responsible for Jurassic–Cretaceous tectonic burial, with Water Canyon anticline in the southern Deep Creek Range located at the top of the thrust zone (e.g., Nelson, 1966; Rodgers, 1987). Note the initial structural position of Hendry’s Creek required for the formation of the staurolite-garnet schist unit (Lewis et al., 1999; Gébelin et al., 2011). (B) Early Eocene collapse of thickened crust, inducing exhumation, flattening, and  $^{40}\text{Ar}/^{39}\text{Ar}$  resetting in the metamorphic units (including Negro Creek). Black dashed lines represent the initial trajectory of the northern Snake Range detachment (NSRD) and associated normal fault system. (C) Initial stages of low-angle detachment faulting (northern Snake Range detachment) and propagation of normal faults within the hanging wall. Normal faults and tension fractures facilitate downward transport of meteoric fluids to the active northern Snake Range detachment footwall. (D) Oligocene–Miocene extension showing the evolution of a rolling hinge with Negro Creek and Hendry’s Creek remaining in the footwall of the developing northern Snake Range detachment. Intensively developed east-dipping normal faults and tension fractures permit circulation of meteoric fluids to the northern Snake Range detachment footwall mylonites (Hendry’s Creek) with high heat flow as driving force for hydrothermal fluid circulation in this part of the northern Snake Range detachment. Note the presence of basins that form directly above the zone of active faulting and connect fluids from the surface to depth. In contrast, along the western flank of the range (Negro Creek), the rolling hinge detachment system induces the rotation and translation of blocks preventing the fluid connection between Earth’s surface and the northern Snake Range detachment footwall.

### Cretaceous crustal shortening

thrusts in Cherry Creek & Antelope Ranges  
Confusion Range folds  
Cretaceous thrust system

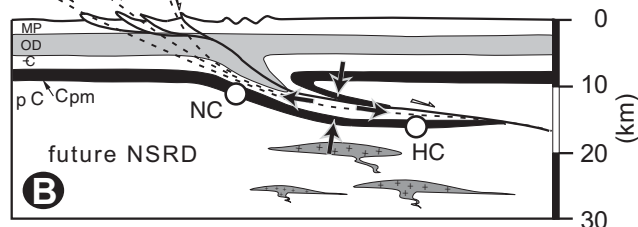
NC: Negro Creek section  
HC: Hendry’s Creek section



### Early Eocene collapse (~49–45 Ma)

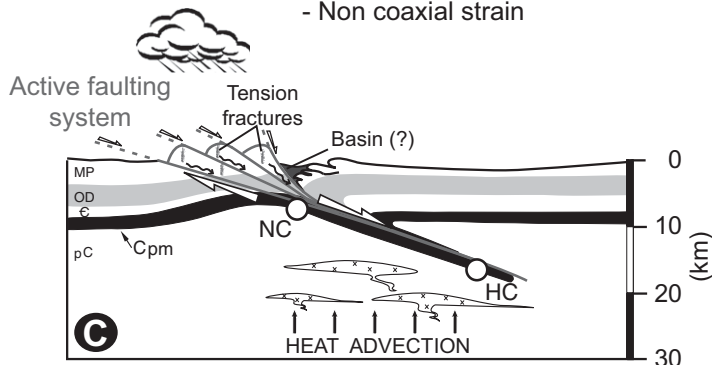
- Crustal thinning
- Coaxial strain

future extensional system



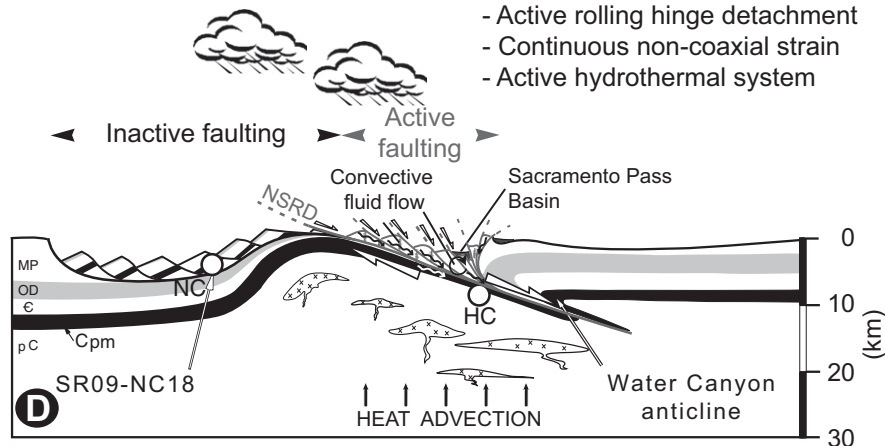
### Early stages of extension

- Detachment development
- Non coaxial strain



### Oligo-Miocene extension (27–21 Ma)

- Active rolling hinge detachment
- Continuous non-coaxial strain
- Active hydrothermal system



### Proposed Model for Northern Snake Range Detachment Evolution

We propose that quartzite observed along the western and eastern flanks of the northern Snake Range metamorphic core complex records two distinct deformation events (Fig. 8). Following Jurassic–Cretaceous crustal shortening, collapse of the thickened Sevier–Laramide hinterland region affected the southern Cordillera from Late Cretaceous to early Eocene time. This extensional event induced a rotation from steep to moderate dip of the west-directed thrust system responsible for tectonic burial of late Precambrian to early Mesozoic strata (Fig. 8A; Lewis et al., 1999). Partial exhumation of the near-horizontal metamorphosed sequence was likely enhanced by Eocene volcanism and plutonism (e.g., Brooks et al., 1995a, 1995b; Henry and Ressel, 2000; Henry, 2008), which heated and softened the crust, facilitating crustal thinning. We suggest that during that time (ca. 49–45 Ma), the Lower Cambrian Prospect Mountain Quartzite and Pioche Shale, which are preserved today along the western flank of the northern Snake Range, experienced coaxial deformation and cooling, with cross-girdle *c*-axis fabric development and Eocene  $^{40}\text{Ar}/^{39}\text{Ar}$  resetting of Cretaceous muscovite (Fig. 8B). In response to lithospheric extension, a moderately dipping brittle-to-ductile normal detachment zone developed and was rooted deeply beneath the thick and rigid foreland region (Fig. 8C). This high-strain zone used the preexisting discontinuity formed by early west-directed thrust systems (Fig. 8B) and localized preferentially in quartzite-dominated lithologies (e.g., Whitney et al., 2013). Moderately to steeply dipping normal faults accommodated extension in the upper brittle crust, producing a fan-shaped fault pattern (e.g., Brun and van den Driessche, 1994). Here, upper-crustal extension generated shear and tension fractures, which enhanced porosity and permeability, with the potential of channelizing surface fluids down to the brittle-ductile transition (Fig. 8C).

As extension proceeded, the detachment zone was rotated toward the horizontal, with the footwall and hanging wall undergoing upward and downward motion, respectively (e.g., Buck, 1988; Brun and van den Driessche, 1994). It is very likely that this rolling-hinge motion was triggered by the presence of low-viscosity material, which flowed in the lower crust to fill the gap created by rotation of the detachment footwall (Whitney et al., 2013).

In accordance with the rolling-hinge model proposed by Buck (1988), Wernicke and Axen (1988), Wernicke (1990), and Brun and van den Driessche (1994), the brittle normal faults that

dissect the upper crust were gradually rotated and translated above the detachment fault and became inactive; in the northern Snake Range detachment, the Negro Creek section may be an example of such a tilted block. In our model, new faults continuously developed in the active wedge of the hanging wall, while footwall rocks were uplifted. The top-to-the-east sheared rocks in the detachment footwall and associated ductile deformation microstructures underwent rapid cooling (Fig. 8D). This rolling-hinge mechanism (e.g., Buck et al., 2005; Smith et al., 2008) explains the characteristic convex-upward shape of the northern Snake Range detachment as well as our  $^{40}\text{Ar}/^{39}\text{Ar}$  and hydrogen isotope results from Hendry's Creek, which indicate a main exhumation event during the Oligocene–Miocene (e.g., Bartley and Wernicke, 1984; Miller et al., 1999a; Gébelin et al., 2011). Continued active faulting along the eastern flank of the detachment permitted fracture-dominated flow of surface fluids down to the brittle-ductile transition (Fig. 8D). This downward flow of surface fluids to the brittle-ductile transition zone was sustained by rapid upward transfer of hot rocks (Gans and Miller, 1983; Miller et al., 1988, 1999a; Gans et al., 1989), which induced buoyancy-driven fluid convection (Person et al., 2007).

The consistently low white mica  $\delta\text{D}$  values from the Hendry's Creek mylonitic quartzite ( $\delta\text{D}_{\text{muscovite}} \sim -150\text{‰}$ ) suggest that meteoric fluids continued to permeate the east-dipping segment of the rolling-hinge detachment. In contrast, meteoric fluid flow may have ceased on the western limb as the rolling-hinge detachment developed and the upper-crust normal faults rotated and became inactive (Brun and van den Driessche, 1994). We note that sample SR09-NC18, collected at the bottom of the Negro Creek section, displays a low  $\delta\text{D}_{\text{muscovite}}$  value ( $\delta\text{D}_{\text{muscovite}} = -142\text{‰}$ ) and a plateau age at 27 Ma, which is consistent with early (late Oligocene) northern Snake Range detachment activity. Therefore, the Negro Creek section may reflect an early stage of fluid connection to the surface that was lost during development of the rolling hinge. In contrast, the mylonitic quartzite at Hendry's Creek recorded cumulative fluid-rock interaction until Miocene time (ca. 21 Ma), with surface fluids that were fed to the detachment zone by numerous brittle normal faults. This style of faulting is well preserved today in the Miocene Sacramento Pass supradetachment basin (Grier, 1984) (Fig. 8D).

In summary, the kinematics of the northern Snake Range rolling-hinge detachment can be associated with progressive fluid flow from the surface to ductile levels of the extending crust. Microstructural, stable isotopic, and thermo-

chronological data suggest that detachment activity started in Oligocene time; this early detachment stage is preserved in the rotated, western flank of the detachment system (Negro Creek section), which also preserves Eocene fabrics. In contrast, continued Miocene hydration of the ductile detachment fabrics on the eastern flank of the detachment system was promoted by active faulting of the upper crust, as observed in the faulted/tilted Sacramento Pass supradetachment basin.

### CONCLUSION

Hydrogen isotope, microstructural, and  $^{40}\text{Ar}/^{39}\text{Ar}$  thermochronology data from the northern Snake Range detachment footwall shed new light on crustal hydrology during extensional tectonics. Oligocene–Miocene extension was accommodated by an east-dipping rolling-hinge detachment system that exhumed detachment footwall rocks in an anticlinal structure of quartzite and schist. The western limb of this anticline was exhumed first and rotated around the rolling hinge. A section of this western limb at Negro Creek preserves Eocene fabrics (49–45 Ma,  $^{40}\text{Ar}/^{39}\text{Ar}$  muscovite ages) that developed during coaxial deformation in the presence of metamorphic fluids. The Eocene fabrics are locally overprinted by late Oligocene shear zones containing muscovite with  $\delta\text{D}$  values characteristic of meteoric water interaction. The eastern flank of the detachment footwall is characterized by intense Oligocene–Miocene (27–21 Ma) ductile deformation and pervasive infiltration of meteoric fluids that likely originated at high elevation ( $\delta\text{D}_{\text{muscovite}} \sim -150\text{‰}$ ). Circulation of meteoric fluids through the brittle-ductile transition was possible by continued faulting of the upper crust on the eastern flank of the detachment during progressive development of the rolling hinge.

More generally, results from this study confirm that rolling-hinge detachments result in diachronous deformation and exhumation patterns as the detachment footwall goes through the rolling hinge. In addition, results suggest that fluid flow is intimately coupled to the porosity-permeability structure that is associated with progressive rolling-hinge deformation (active faults, faults rendered inactive by rotation), and exhumation. Sustained fluid flow through the upper crust and hydration of the ductile crust by meteoric fluids are expected in the downdip direction of a rolling-hinge detachment.

### ACKNOWLEDGMENTS

This study was funded through the LOEWE program of Hesse's Ministry of Higher Education, Research, and the Arts and additional support through a

Leibniz University Hannover young investigator grant “Wege in die Forschung” to Gébelin and National Science Foundation grant EAR-0838541 to Teyssier. Mulch acknowledges support through EAR-1019648. We thank F. Barou (University of Montpellier) for electron backscatter diffraction support. We acknowledge the very insightful and careful remarks of B. Ábalos, an anonymous reviewer, and Associate Editor B. Grasemann, which clarified and improved the manuscript.

## REFERENCES CITED

- Abalos, B., 1997, Omphacite fabric variation in the Cabo Ortegal Eclogite (NW Spain): relationship with strain symmetry during high pressure deformation: *Journal of Structural Geology*, v. 19, p. 621–637, doi:10.1016/S0191-8141(97)00001-1.
- Armstrong, R.L., 1972, Low-angle (denudation) faults, hinterland of the Sevier orogenic belt, eastern Nevada and western Utah: *Geological Society of America Bulletin*, v. 83, p. 1729–1754, doi:10.1130/0016-7606(1972)83<1729:LDFHOT>2.0.CO;2.
- Armstrong, R.L., and Hansen, E., 1966, Cordilleran infrastructure in the eastern Great Basin: *American Journal of Science*, v. 264, p. 112–127, doi:10.2475/ajs.264.2.112.
- Bartley, J.M., and Wernicke, B.P., 1984, The Snake Range décollement interpreted as a major extensional shear zone: *Tectonics*, v. 3, p. 647–657, doi:10.1029/TC003i006p0647.
- Brooks, W.E., Thorman, W.E., and Snee, L.W., 1995a, The <sup>40</sup>Ar/<sup>39</sup>Ar ages and tectonic setting of the middle Eocene northeast Nevada volcanic field: *Journal of Geophysical Research*, v. 100, p. 10,403–10,416, doi:10.1029/94JB03389.
- Brooks, W.E., Thorman, W.E., Snee, L.W., Nutt, C.W., Potter, C.J., and Dubiel, R.F., 1995b, Summary of Chemical Analyses and <sup>40</sup>Ar/<sup>39</sup>Ar-Spectra Data for Eocene Volcanic Rocks from the Central Part of the Northeast Nevada Volcanic Field: U.S. Geological Survey Bulletin 1988-K, p. K1–K33.
- Brun, J.-P., and van den Driessche, J., 1994, Extensional gneiss domes and detachment fault systems—Structure and kinematics: *Bulletin de la Société Géologique de France*, v. 165, p. 519–530.
- Buck, W.R., 1988, Flexural rotation of normal faults: *Tectonics*, v. 7, p. 959–973, doi:10.1029/TC007i005p0959.
- Buck, W.R., Lavier, L.L., and Poliakov, A.N.B., 2005, Modes of faulting at mid-ocean ridges: *Nature*, v. 434, p. 719–723, doi:10.1038/nature03358.
- Bunge, H.J., 1982, Texture Analysis in Material Science: London, Butterworths, 616 p.
- Coney, P.J., 1974, Structural analysis of the Snake Range “décollement,” east-central Nevada: *Geological Society of America Bulletin*, v. 88, p. 1237–1250.
- Coney, P.J., 1980, Cordilleran metamorphic core complexes: An overview, in Crittenden, M.D., Coney, P.J., and Davis, G.H., eds., *Cordilleran Metamorphic Core Complexes*: Geological Society of America Memoir 153, p. 7–34.
- Davis, G.H., and Coney, P.J., 1979, Geologic development of the Cordilleran metamorphic core complexes: *Geology*, v. 7, p. 120–124, doi:10.1130/0091-7613(1979)7<120:GDOTCM>2.0.CO;2.
- Dunlap, W.J., 1992, Structure, Kinematics, and Cooling History of the Arltunga Nappe Complex, Central Australia [Ph.D. thesis]: Minneapolis, Minnesota, University of Minnesota, 276 p.
- Fricke, H.C., Wickham, S.M., and O’Neil, J.R., 1992, Oxygen and hydrogen isotope evidence for meteoric water infiltration during mylonitization and uplift in the Ruby Mountains–East Humboldt Range core complex, Nevada: *Contributions to Mineralogy and Petrology*, v. 111, p. 203–221, doi:10.1007/BF00348952.
- Gans, P.B., and Miller, E.L., 1983, Style of mid-Tertiary extension in east-central Nevada, in Gurgel, K.D., ed., *Geologic Excursions in the Overthrust Belt and Metamorphic Core Complexes of the Intermountain Region*: Utah Geological and Mineral Survey Special Studies Guidebook 59, Part 1, p. 107–160.
- Gans, P.B., Miller, E.L., McCarthy, J., and Oldcott, M.L., 1985, Tertiary extensional faulting and evolving ductile-brittle transition zones in the northern Snake Range and vicinity: New insights from seismic data: *Geology*, v. 13, p. 189–193, doi:10.1130/0091-7613(1985)13<189:TEFAED>2.0.CO;2.
- Gans, P.B., Mahood, G.A., and Schermer, E., 1989, Synextensional Magmatism in the Basin and Range Province: A Case Study from the Eastern Great Basin: Geological Society of America Special Paper 223, 53 p.
- Gans, P., Miller, E.L., and Lee, J., 1999a, Preliminary Geologic Map of the Spring Mountain 7.5’ Quadrangle, Northern Snake Range, Nevada-Utah: Nevada Bureau of Mines and Geology Field Studies Map 18, scale 1:24,000.
- Gans, P.B., Miller, E.L., Huggins, C.C., and Lee, J., 1999b, Preliminary Geologic Map of the Little Horse Canyon 7.5’ Quadrangle, Nevada and Utah: Nevada Bureau of Mines and Geology Field Studies Map 20, scale 1:24,000.
- Gébelin, A., Mulch, A., Teyssier, C., Heizler, M., Vennemann, T., and Seaton, N.C.A., 2011, Oligo-Miocene extensional tectonics and fluid flow across the northern Snake Range detachment system, Nevada: *Tectonics*, v. 30, p. 1–18, TC5010, doi:10.1029/2010TC002797.
- Gébelin, A., Mulch, A., Teyssier, C., Chamberlain, C.P., and Heizler, M., 2012, Coupled basin-detachment systems as paleoaltimetry archives of the western North American Cordillera: *Earth and Planetary Science Letters*, v. 335–336, p. 36–47, doi:10.1016/j.epsl.2012.04.029.
- Gébelin, A., Mulch, A., Teyssier, C., Jessup, M.J., Law, R.D., and Brunel, M., 2013, The Miocene elevation of Mount Everest: *Geology*, v. 41, p. 799–802, doi:10.1130/G34331.1.
- Gottardi, R., Teyssier, C., Mulch, A., Vennemann, T.W., and Wells, M.L., 2011, Preservation of extreme transient geotherm in the Raft River detachment shear zone: *Geology*, v. 39, no. 8, p. 759–762, doi:10.1130/G31834.1.
- Gottardi, R., Kao, P.H., Saar, M.O., and Teyssier, C., 2013, Effects of permeability fields on fluid, heat, and oxygen isotope transport in extensional detachment systems: *Geochemistry Geophysics Geosystems*, v. 14, p. 1493–1522, doi:10.1002/ggge.20100.
- Grier, S.P., 1984, Alluvial Fan and Lacustrine Carbonate Deposits in the Snake Range: A Study of Tertiary Sedimentation and Associated Tectonism [M.S. thesis]: Stanford, California, Stanford University, 61 p.
- Henry, C.D., 2008, Ash-flow tuffs and paleovalleys in north-eastern Nevada: Implications for Eocene paleogeography and extension in the Sevier hinterland, northern Great Basin: *Geosphere*, v. 4, no. 1, p. 1–35, doi:10.1130/GES00122.1.
- Henry, C.D., and Ressel, M.W., 2000, Eocene Magmatism and its Role in Generating Sediment Hosted Gold Deposits of the Carlin Trend: Geological Society of Nevada Symposium 2000 Field Trip Guidebook 4, 223 p.
- Hirth, G., and Tullis, J., 1992, Dislocation creep regimes in quartz aggregates: *Journal of Structural Geology*, v. 14, p. 145–159, doi:10.1016/0191-8141(92)90053-Y.
- Hose, R.K., and Blake, M.C., 1976, Geology and Mineral Resources of White Pine County, Nevada, Part 1, Geology: Nevada Bureau of Mines and Geology Bulletin 85, p. 1–35, scale 1:250,000.
- Jessell, M.W., 1987, Grain-boundary migration microstructures in a naturally deformed quartzite: *Journal of Structural Geology*, v. 9, p. 1007–1014, doi:10.1016/0191-8141(87)90008-3.
- Lee, D.E., Marvin, R.F., Stern, T.W., and Peterman, Z.E., 1970, Modification of Potassium-Argon Ages by Tertiary Thrusting in the Snake Range, White Pine County, Nevada: U.S. Geological Survey Professional Paper 700-D, p. D92–D102.
- Lee, D.E., Marvin, R.F., and Mehnert, H.H., 1980, A Radiometric Age Study of Mesozoic–Cenozoic Metamorphism in Eastern White Pine County, Nevada, and Nearby Utah: U.S. Geological Survey Professional Paper 1158-C, p. 17–28.
- Lee, J., 1995, Rapid uplift and rotation of mylonitic rocks from beneath a detachment fault: Insights from potassium feldspar <sup>40</sup>Ar/<sup>39</sup>Ar thermochronology, northern Snake Range, Nevada: *Tectonics*, v. 14, p. 54–77, doi:10.1029/94TC01508.
- Lee, J., and Sutter, J.F., 1991, Incremental <sup>40</sup>Ar/<sup>39</sup>Ar thermochronology of mylonitic rocks from the northern Snake Range, Nevada: *Tectonics*, v. 10, p. 77–100, doi:10.1029/90TC01931.
- Lee, J., Miller, E.L., and Sutter, J.F., 1987, Ductile strain and metamorphism in an extensional tectonic setting: A case study from the northern Snake Range, Nevada, USA, in Coward, M.P., Dewey, J.F., and Hancock, P.L., eds., *Continental Extensional Tectonics*: Geological Society of London Special Publication 28, p. 267–298.
- Lee, J., Gans, P.B., and Miller, E.L., 1999a, Preliminary Geologic Map of the Mormon Jack Pass 7.5’ Quadrangle, Northern Snake Range, White Pine County, Nevada: Nevada Bureau of Mines and Geology Field Studies Map 17, scale 1:24,000.
- Lee, J., Gans, P.B., and Miller, E.L., 1999b, Preliminary Geologic Map of the Third Butte East 7.5’ Quadrangle, Northern Snake Range, White Pine County, Nevada: Nevada Bureau of Mines and Geology Field Studies Map 16, scale 1:24,000.
- Lee, J., Miller, E.L., Gans, P.B., and Huggins, C.C., 1999c, Preliminary Geologic Map of the Mount Moriah 7.5’ Quadrangle, Northern Snake Range, White Pine County, Nevada: Nevada Bureau of Mines and Geology Field Studies Map 19, scale 1:24,000.
- Lewis, C.J., Wernicke, B.P., Selverstone, J., and Bartley, J.M., 1999, Deep burial of the footwall of the northern Snake Range décollement, Nevada: *Geological Society of America Bulletin*, v. 111, p. 39–51, doi:10.1130/0016-7606(1999)111<0039:DBOTFO>2.3.CO;2.
- Lister, G.S., 1977, Discussion: Crossed-girdle c-axis fabrics in quartzites plastically deformed by plane strain and progressive simple shear: *Tectonophysics*, v. 39, p. 51–54, doi:10.1016/0040-1951(77)90087-7.
- Lister, G.S., and Davis, G.A., 1989, The origin of metamorphic core complexes and detachment faults formed during Tertiary continental extension in the northern Colorado River region, USA: *Journal of Structural Geology*, v. 11, p. 65–94, doi:10.1016/0191-8141(89)90036-9.
- Losh, S., 1997, Stable isotope and modeling studies of fluid-rock interaction associated with the Snake Range and Mormon Peak detachment faults, Nevada: *Geological Society of America Bulletin*, v. 109, p. 300–323, doi:10.1130/0016-7606(1997)109<0300:SIAMSO>2.3.CO;2.
- Mainprice, D., 2005, Pfch5 (computer software): [ftp://www.gm.univ-montp2.fr/mainprice/Care-Ware\\_Unicef\\_Programs/](ftp://www.gm.univ-montp2.fr/mainprice/Care-Ware_Unicef_Programs/) (accessed 28 May 2014).
- Mainprice, D.H., and Paterson, M.S., 1984, Experimental studies of the role of water in the plasticity of quartzites: *Journal of Geophysical Research*, v. 89, p. 4257–4269, doi:10.1029/JB089iB06p04257.
- Miller, E.L., and Gans, P.B., 1989, Cretaceous crustal structure and metamorphism in the hinterland of the Sevier thrust belt, western U.S. Cordillera: *Geology*, v. 17, p. 59–62, doi:10.1130/0091-7613(1989)017<0059:CCSAMI>2.3.CO;2.
- Miller, E.L., and Gans, P.B., 1999, Preliminary Geologic Map of the Cove 7.5’ Quadrangle, Northern Snake Range, White Pine County, Nevada: Nevada Bureau of Mines and Geology Field Studies Map 22, scale 1:24,000.
- Miller, E.L., Gans, P.B., and Garing, J.D., 1983, The Snake Range décollement: An exhumed mid-Tertiary ductile-brittle transition: *Tectonics*, v. 2, p. 239–263, doi:10.1029/TC002i003p0239.
- Miller, E.L., Gans, P.B., Wright, J.E., and Sutter, J.F., 1988, Metamorphic history of the east-central Basin and Range Province: Tectonic setting and relationship to magmatism, in Ernst, W.G., ed., *Metamorphism and Tectonic Evolution of the Western U.S. Cordillera (Rubey Volume VII)*: Englewood Cliffs, New Jersey, Prentice-Hall, p. 649–682.
- Miller, E.L., Dumitru, T.A., Brown, R.W., and Gans, P.B., 1999a, Rapid Miocene slip on the Snake Range–Deep Creek Range fault system, east-central Nevada: *Geological Society of America Bulletin*, v. 111, p. 886–905, doi:10.1130/0016-7606(1999)111<0886:RMSOTS>2.3.CO;2.
- Miller, E.L., Gans, P.B., Grier, S.P., Huggins, C.C., and Lee, J., 1999b, Preliminary Geologic Map of the Old

- Mans Canyon 7.5' Quadrangle, Northern Snake Range, White Pine County, Nevada: Nevada Bureau of Mines and Geology Field Studies Map 21, scale 1:24,000.
- Mulch, A., Teyssier, C., Cosca, M.A., Vanderhaeghe, O., and Vennemann, T., 2004, Reconstructing paleoelevation in eroded orogens: *Geology*, v. 32, p. 525–528, doi:10.1130/G20394.1.
- Mulch, A., Cosca, M.A., Fiebig, J., and Andresen, A., 2005, Time scales of mylonitic deformation and meteoric fluid infiltration during extensional detachment faulting: An integrated in situ <sup>40</sup>Ar/<sup>39</sup>Ar geochronology and stable isotope study of the Porsgrunn-Kristiansand shear zone (southern Norway): *Earth and Planetary Science Letters*, v. 233, p. 375–390, doi:10.1016/j.epsl.2005.01.042.
- Mulch, A., Teyssier, C., Cosca, M.A., and Vennemann, T., 2006, Thermomechanical analysis of strain localization in a detachment zone: *Journal of Geophysical Research*, v. 111, p. 1–20, doi:10.1029/2005JB004032.
- Nelson, R.B., 1966, Structural development of northernmost Snake Range, Kern Mountains, and Deep Creek Range, Nevada and Utah: *The American Association of Petroleum Geologists Bulletin*, v. 50, p. 921–951.
- Nesbitt, B.E., and Muehlenbachs, K., 1995, Geochemistry of syntectonic, crustal fluid regimes along the Lithoprobe southern Canadian Cordillera transect: *Canadian Journal of Earth Sciences*, v. 32, p. 1699–1719, doi:10.1139/e95-134.
- Person, M., Mulch, A., Teyssier, C., and Gao, Y., 2007, Isotope transport and exchange within metamorphic core complexes: *American Journal of Science*, v. 307, p. 555–589, doi:10.2475/03.2007.01.
- Rodgers, D.W., 1987, Thermal and Structural Evolution of the Southern Deep Creek Range, West-Central Utah and East-Central Nevada [Ph.D. dissertation]: Stanford, California, Stanford University, 149 p.
- Smith, D.K., Escartin, J., Schouton, H., and Cann, J.R., 2008, Fault rotation and core complex formation: Significant processes in seafloor formation at slow spreading mid-ocean ridges (Mid-Atlantic Ridge, 13–15°N): *Geochemistry Geophysics Geosystems*, v. 9, no. 3, doi:10.1029/2007GC001699.
- Stewart, J.H., 1980, *Geology of Nevada*: Nevada Bureau of Mines and Geology Special Publication 4, 136 p.
- Suzuoki, T., and Epstein, S., 1976, Hydrogen isotope fractionation between OH-bearing minerals and water: *Geochimica et Cosmochimica Acta*, v. 40, p. 1229–1240, doi:10.1016/0016-7037(76)90158-7.
- Taylor, H.P., 1990, Oxygen and hydrogen isotope constraints on the deep circulation of surface waters into zones of hydrothermal metamorphism and melting, in *Geophysics Study Committee, National Research Council. The Role of Fluids in Crustal Processes*: Washington, D.C.: The National Academies Press, p. 72–95.
- Ten Grotenhuis, S.M., Trouw, R.A.J., and Passchier, C.W., 2003, Evolution of mica fish in mylonitic rocks: *Tectonophysics*, v. 372, p. 1–21, doi:10.1016/S0040-1951(03)00231-2.
- Tullis, J., Christie, J.M., and Griggs, D.T., 1973, Microstructures and preferred orientations in experimentally deformed quartzites: *Geological Society of America Bulletin*, v. 84, p. 297–314, doi:10.1130/0016-7606(1973)84<297:MAPOOE>2.0.CO;2.
- Ulrich, S., and Mainprice, D., 2005, Does cation ordering in omphacite influence development of lattice preferred orientation?: *Journal of Structural Geology*, v. 27, p. 419–431, doi:10.1016/j.jsg.2004.11.003.
- Vollmer, F., 1990, An application of eigenvalue methods to structural domain analysis: *Geological Society of America Bulletin*, v. 102, p. 786–791, doi:10.1130/0016-7606(1990)102<0786:AAOEMT>2.3.CO;2.
- Wernicke, B., 1981, Low-angle normal faults in the Basin and Range Province: Nappe tectonics in an extending orogeny: *Nature*, v. 291, p. 645–648, doi:10.1038/291645a0.
- Wernicke, B., 1990, The fluid crustal layer and its implications for continental dynamics, in *Salisbury, M.H., and Fountain, D., eds., Exposed Cross-Sections of Continental Crust*: Dordrecht, Netherlands, Kluwer, p. 509–544.
- Wernicke, B., and Axen, G.J., 1988, On the role of isostasy in the evolution of normal fault systems: *Geology*, v. 16, p. 848–851, doi:10.1130/0091-7613(1988)016<0848:OTROI>2.3.CO;2.
- Whitebread, D.H., 1969, *Geologic Map of the Wheeler Peak and Garrison Quadrangles, Nevada and Utah*: U.S. Geological Survey Miscellaneous Investigations Map I-578, scale 1:48,000, 7 p.
- Whitney, D.L., Teyssier, C., Rey, P., and Buck, W.R., 2013, Continental and oceanic core complexes: *Geological Society of America Bulletin*, v. 125, p. 273–298, doi:10.1130/B30754.1.
- Wilson, C.J.L., and Bell, I.A., 1979, Deformation of biotite and muscovite: *Tectonophysics*, v. 58, p. 179–200, doi:10.1016/0040-1951(79)90328-7.
- Wright, L.A., Otton, J.K., and Troxel, B.W., 1974, Turtleback surfaces of Death Valley viewed as phenomena of extension: *Geology*, v. 2, p. 53–54, doi:10.1130/0091-7613(1974)2<53:TSODVV>2.0.CO;2.

SCIENCE EDITOR: DAVID SCHOFIELD  
ASSOCIATE EDITOR: BERNHARD GRASEMANN

MANUSCRIPT RECEIVED 9 JANUARY 2014  
REVISED MANUSCRIPT RECEIVED 23 MAY 2014  
MANUSCRIPT ACCEPTED 1 JULY 2014

Printed in the USA

## Geological Society of America Bulletin

### Meteoric water circulation in a rolling-hinge detachment system (northern Snake Range core complex, Nevada)

Aude G ebelin, Christian Teyssier, Matthew T. Heizler and Andreas Mulch

*Geological Society of America Bulletin* 2015;127, no. 1-2;149-161  
doi: 10.1130/B31063.1

---

#### Email alerting services

click [www.gsapubs.org/cgi/alerts](http://www.gsapubs.org/cgi/alerts) to receive free e-mail alerts when new articles cite this article

#### Subscribe

click [www.gsapubs.org/subscriptions/](http://www.gsapubs.org/subscriptions/) to subscribe to Geological Society of America Bulletin

#### Permission request

click <http://www.geosociety.org/pubs/copyrt.htm#gsa> to contact GSA

Copyright not claimed on content prepared wholly by U.S. government employees within scope of their employment. Individual scientists are hereby granted permission, without fees or further requests to GSA, to use a single figure, a single table, and/or a brief paragraph of text in subsequent works and to make unlimited copies of items in GSA's journals for noncommercial use in classrooms to further education and science. This file may not be posted to any Web site, but authors may post the abstracts only of their articles on their own or their organization's Web site providing the posting includes a reference to the article's full citation. GSA provides this and other forums for the presentation of diverse opinions and positions by scientists worldwide, regardless of their race, citizenship, gender, religion, or political viewpoint. Opinions presented in this publication do not reflect official positions of the Society.

---

#### Notes